Synthesis B. Musio et al. Paper

Combination of Enabling Technologies to Improve and Describe the Stereoselectivity of Wolff–Staudinger Cascade Reaction

B. Musio[a]
F. Mariani[a,b]
E. P. Śliwiński[a]
M. A. Kabeshov[a]
H. Odajima[c]
S. V. Ley*[a]

[a] University of Cambridge, Department of Chemistry, Lensfield Road, Cambridge, CB2 1EW, UK
svl1000@cam.ac.uk
[b] Universitat de Barcelona, Laboratori de Química Orgànica, Facultat de Farmàcia, Av. Joan XXIII s/n, 08028 Barcelona, Spain
[c] Saida FDS, 143-10 Itsushiki, Yaizu-shi, Shizuoka Prefecture 4250054, Japan

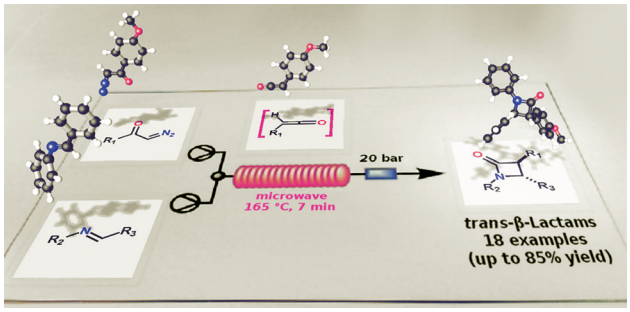

Received: 11.07.2016
Accepted after revision: 07.08.2016
Published online: 10.08.2016
DOI: 10.1055/s-0035-1562579; Art ID: ss-2016-z0490-op

Abstract A new, single-mode bench-top resonator was evaluated for the microwave-assisted flow generation of primary ketenes by thermal decomposition of α-diazoketones at high temperature. A number of amides and β-lactams were obtained by ketene generation *in situ* and reaction with amines and imines, respectively, in good to excellent yields. The preferential formation of *trans*-configured β-lactams was observed during the [2+2] Staudinger cycloaddition of a range of ketenes with different imines under controlled reaction conditions. Some insights into the mechanism of this reaction at high temperature are reported, and a new web-based molecular viewer, which takes advantage from Augmented Reality (AR) technology, is also described for a faster interpretation of computed data.

Key words microwave, Wolff, Staudinger, flow, Augmented Reality, molecular visualisation

There is a considerable interest in developing more energy efficient, safer and more flexible chemical processes, which meet competitive sustainability challenges.[1] Microreactor technology and flow chemistry can be considered under the umbrella of strategies for process intensification,[2] as demonstrated by their popularity both in academia and in industry.[3] More importantly, the possibility of combining continuous-flow technology with other enabling technologies leads to autonomous processes and increased throughput.[4] There is now a plethora of examples describing the advantages arising from the combination of flow chemistry with heterogeneous catalysis,[5] photochemistry,[6] electrochemistry,[7] ultrasound,[8] etc.

In particular, high temperature and high pressure chemical transformations can be derived from the synergic benefits of microwave irradiation[9] and continuous-flow technology,[10] as demonstrated by several applications reported during the last decade.[11] Indeed, the traditional batch-type microwave chemistry suffers from lack of reproducibility during scale-up, owing to increased heat loss, changes in absorption, limited penetration depth of the radiation and additional reflection of the microwaves.[12] Since the first-generation of *flow-microwave* reactor introduced in 1990,[13] great efforts have been made to design modern flow microwave reactors that could be applied to industrial scale.[14] In particular, some of the instruments introduced so far are defined by high level of control, reproducibility and safety, thanks to the integration of accurate temperature and pressure monitoring. Nevertheless, further research is needed to improve the energy efficiency, the capacity, the temperature and pressure window of operation, and the cost of any newly introduced microwave flow reactor.

Herein, we wish to report a new multidisciplinary approach to solve a chemical synthesis problem by using a combined armoury of some new enabling technologies to achieve sustained high-temperature processes with improved reaction selectivity, which can be mechanistically rationalised through computational methods and finally visualised by a new web-based molecular viewer employing Augmented Reality (AR) technology. While most publications to date choose to isolate these individual components, we feel that many synergistic benefits accrue by taking a more holistic modern approach to a problem.

The well-known and extensively studied Wolff–Staudinger reactions to afford β-lactams *via* [2+2] cycloaddition of ketenes with imines is a case in point. While achievable under a variety of conditions with a wide substrate scope, stereoselectivity and scale-up can be problematic for this transformation. In particular, the high temperature and release of gaseous nitrogen as a by-product upon Wolff rearrangement of α-diazocarbonyl compounds to produce intermediate ketenes is seen as a hazardous transformation[15] despite the value of the final β-lactam cycloaddition products.

In the first phase of the program we examined the heating efficiency of a recently developed single-mode benchtop continuous-flow microwave apparatus[16] for the improved generation of primary ketenes from α-diazoketones by Wolff rearrangement at high temperature. We tested the reproducibility of the equipment to function over an extended period of time, monitoring some crucial parameters in real time. A good ratio between the irradiating power and the reflecting power was observed, showing a good efficiency of the system in maintaining constant field strength (Figure 1a).[17]

Pressure regulators installed in front and back-end of the flow borosilicate glass reactor allowed an accurate control of the pressure inside the system (Figure 1b). The monitoring of the temperature under classical sealed-vessel microwave conditions is often not easy, because classical direct temperature sensors such as thermometers or thermocouples can interfere with the electromagnetic field.[18] In our flow microwave set-up, the temperature inside the reactor could be continuously monitored by using a thermocouple installed at the exit of the coil, without affecting the uniformity of the electromagnetic field. Once the steady state was reached, an impressive stability of the temperature was recorded (Figure 1c). The maximum temperature reached was dependent on the irradiating power and on the residence time of the solution inside the irradiating cavity. The steady state was reached faster at higher flow rate, thus at low residence time (Figure 1d). This is in accordance with the reported studies on the efficiency of energy transfer of the microwave irradiation into heat, which can be affected by the additional reflection of the microwaves inside the irradiation cavity.[17] To assess the reliability of the temperature measurement by the thermocouple, a sequence of thermal images were captured over the time. For this purpose, a thermal camera was directed at a slit positioned on one wall of the microwave cavity, containing the reactor tube. A uniform temperature distribution was reached after a few minutes throughout the borosilicate glass reactor (for more details see the Supporting Information).

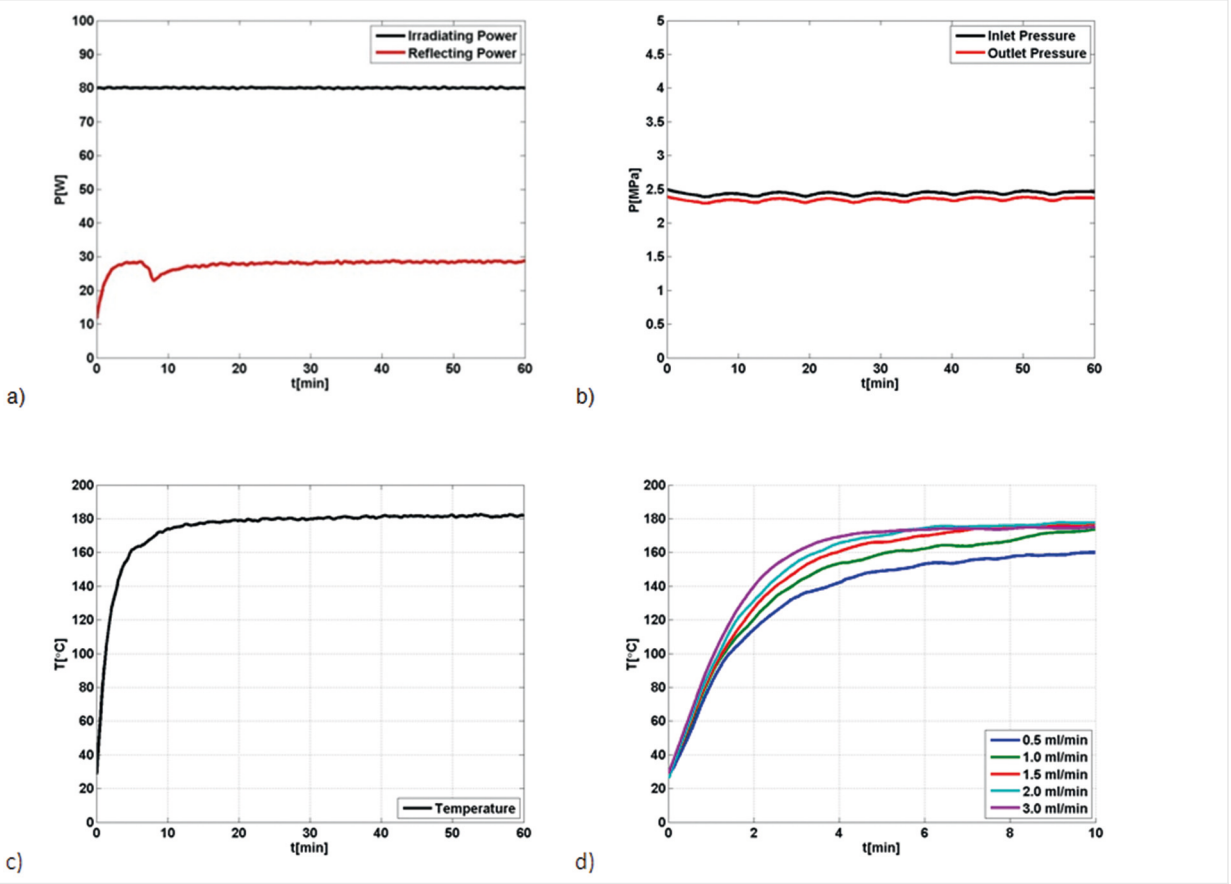

Figure 1 (a) Irradiating power and reflecting power over 1 h. Solvent: acetonitrile; flow rate: 1.0 mL/min; back pressure regulator (BPR): 20 bar. (b) Inlet pressure and outlet pressure over 1 h. Solvent: acetonitrile; flow rate: 1.0 mL/min; back pressure regulator (BPR): 20 bar. (c) Temperature measured by a thermocouple at the exit of the reactor over 1 h. Solvent: acetonitrile; flow rate: 1.0 mL/min; back pressure regulator (BPR): 20 bar. (d) Temperature measured by a thermocouple at the exit of the reactor at different flow rate (0.5, 1.0, 1.5, 2.0 and 3.0 mL/min). Solvent: acetonitrile; back pressure regulator (BPR): 20 bar.

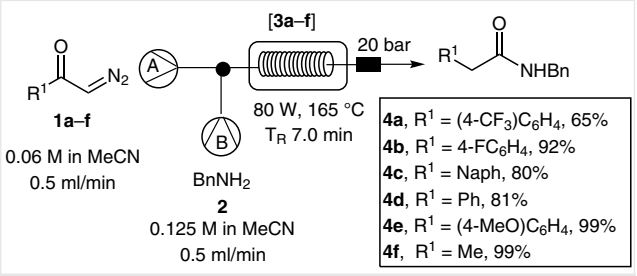

Scheme 1 Continuous-flow microwave-assisted Wolff rearrangement of α-diazoketones **1a–f** and trapping of ketene **3a–f** *in situ* with benzylamine **2**.

The new equipment was applied to the generation of ketene from α-diazoketone followed by trapping *in situ* with benzylamine (Scheme 1). The solvent, the reagent concentration, the irradiation power and the flow rate were accurately adjusted to reduce collateral reactions arising from the extremely high reactivity of the heated ketenes.[19] The best results were observed when the reaction mixture in acetonitrile was passed through the reactor at 1.0 mL/min and heated at 165 °C by irradiating with a power of 80 W. Thus a solution (0.06 M in acetonitrile) of different α-diazoketones **1a–f** was pumped and then mixed with a solution of benzylamine **2** (0.125 M in acetonitrile) before passing through the helical tubular borosilicate glass reactor contained in the microwave cavity. The resulting amides **4a–f** were isolated in good yields (65–99%) after passing through the reactor at 1 mL/min (residence time = 7 minutes) and heated at 165 °C by 80 W irradiation.

The safety and the reliability of the system during the reaction scale-up were evaluated by attempting a continuous multigram synthesis of amide **4f**. The crucial parameters (temperature and pressure) were stable over the reaction time, and the preparation of **4f** was accomplished in 7 h, with no need for further purification (15 mmol, 2.4 g).

Interestingly, similar results were not observed when the same reaction was performed under standard sealed vessel microwave conditions. Attempts to generate the ketenes through more conventional conductive heating in flow were also performed. The reagent mixture was passed continuously through a stainless steel coil under different reaction conditions (solvent, temperature, flow rate). In all the cases, both lower conversion and poorer selectivity were observed, thereby further demonstrating the efficiency of the new microwave flow set-up. Our group recently reported on the flow reaction of imines with mono-alkyl and phenyl ketenes, generated by zinc-mediated dehalogenation of α-bromo acyl bromides at room temperature, to provide β-lactams. The final products were obtained in good yields but with variable diastereomeric ratios.[20] In an attempt to demonstrate the beneficial effect of a rapid microwave-assisted heating of the reagents, we decided to apply the above protocol of the Wolff generated ketenes in combination with a Staudinger cycloaddition reaction particularly with regard to the stereoselective outcome. A number of differently substituted α-diazoketones and imines were reacted under the above optimised reaction conditions for the synthesis of amides (solvent: MeCN; flow rate 0.5 mL/min per pump; irradiating power: 80 W; temperature: 165 °C).

When aliphatic, aryl and heteroaryl α-diazoketones **1e–i** were reacted with *N*-benzylidene benzylamine (*E*)-**5a**, a range of β-lactams **6a–e** were obtained in good yields (up to 85%) and with high comparable diastereoselectivity (Scheme 2).

The specific substitution pattern of the imine was also evaluated by reacting imines (*E*)-**5a–m** with one specific α-diazoketone **1e**, affording β-lactams **6a** and **6g–r** (13 examples, Scheme 2). A preferential formation of *trans*-configured β-lactams was observed in all these cases, with the exception of **6j** (dr *trans*/*cis* 1:16.4), **6k** (dr *trans*/*cis* 1.1:1) and **6r** (dr *trans*/*cis* 1:1). The size of the substituent at the nitrogen atom of the imine likely affected the stereochemical outcome of the [2+2] Staudinger cycloaddition. The preferential formation of *trans*-configured β-lactams was observed for **6g** (R^2 = Me) and **6h** (R^2 = *n*-Bu). When imine (*E*)-**5d** (R^2 = *i*-Pr, R^3 = Ph) was reacted with ketene **1e**, β-lactam **6i** was formed as a mixture of *trans*- and *cis*-configured products (dr *trans*/*cis* 3.2:1). Interestingly, when the imine (*E*)-**5e** (R^2 = *t*-Bu, R^3 = Ph), containing a bigger substituent at the nitrogen atom, was reacted with **1e**, the formation of the β-lactam **6j** proceeded stereoselectively in favour of the *cis*-configured product (dr *trans*/*cis* 1:16.4). Similar effect of the size of the substituent at the nitrogen of the imine was observed during the formation of *N*-benzyl β-lactams **6a** and **6r**. The [2+2] Staudinger cycloaddition reaction proceeded stereoselectively (dr *trans*/*cis* 24:1) and in high yields (85%) for **1e** (R^1 = (4-MeO)C_6H_4) with (*E*)-**5a** (R^2 = Bn, R^3 = Ph), giving **6a**. In contrast, β-lactam **6r** was obtained in poor yield (30%) and with no diastereoselectivity (dr *trans*/*cis* 1:1) by reaction of **1e** [R^1 = (4-MeO)C_6H_4] with (*E*)-**5m** (R^2 = $CHPh_2$, R^3 = Ph).

The effect of the substitution at the sp^2 carbon of the imine was also considered, reacting diazoketone **1e** with different *N*-benzylideneimines (*E*)-**5g–j** under our conditions. When the electron-rich imine (*E*)-**5i** (R^2 = Ph, R^3 = (4-MeO)C_6H_4) was reacted with **1e**, β-lactam **6m** was obtained in good yield (61%) and high diastereomeric ratio (dr *trans*/*cis* 9:1). However, when electron-poor imines (*E*)-**5g** (R^2 = Ph, R^3 = pyridin-2-yl) and (*E*)-**5j** [R^2 = Ph, R^3 = (4-FC_3)C_6H_4] were employed under the same reaction conditions, the resulting β-lactams **6l** and **6o** were formed in lower yields (respectively 56% and 47%) and lower diastereomeric ratio (respectively dr *trans*/*cis* 3.8:1 for **6l** and 5:1 for **6o**). To demonstrate the additive effect of the substitution at the nitrogen atom and the substituent at the sp^2 carbon of the imine, ketene **1e** was reacted with imine (*E*)-**5f** (R^2 = *i*-Pr, R^3 = pyridin-2-yl). The resulting β-lactam **6k** was obtained with low diastereoselectivity (dr *trans*/*cis* 1.1:1),

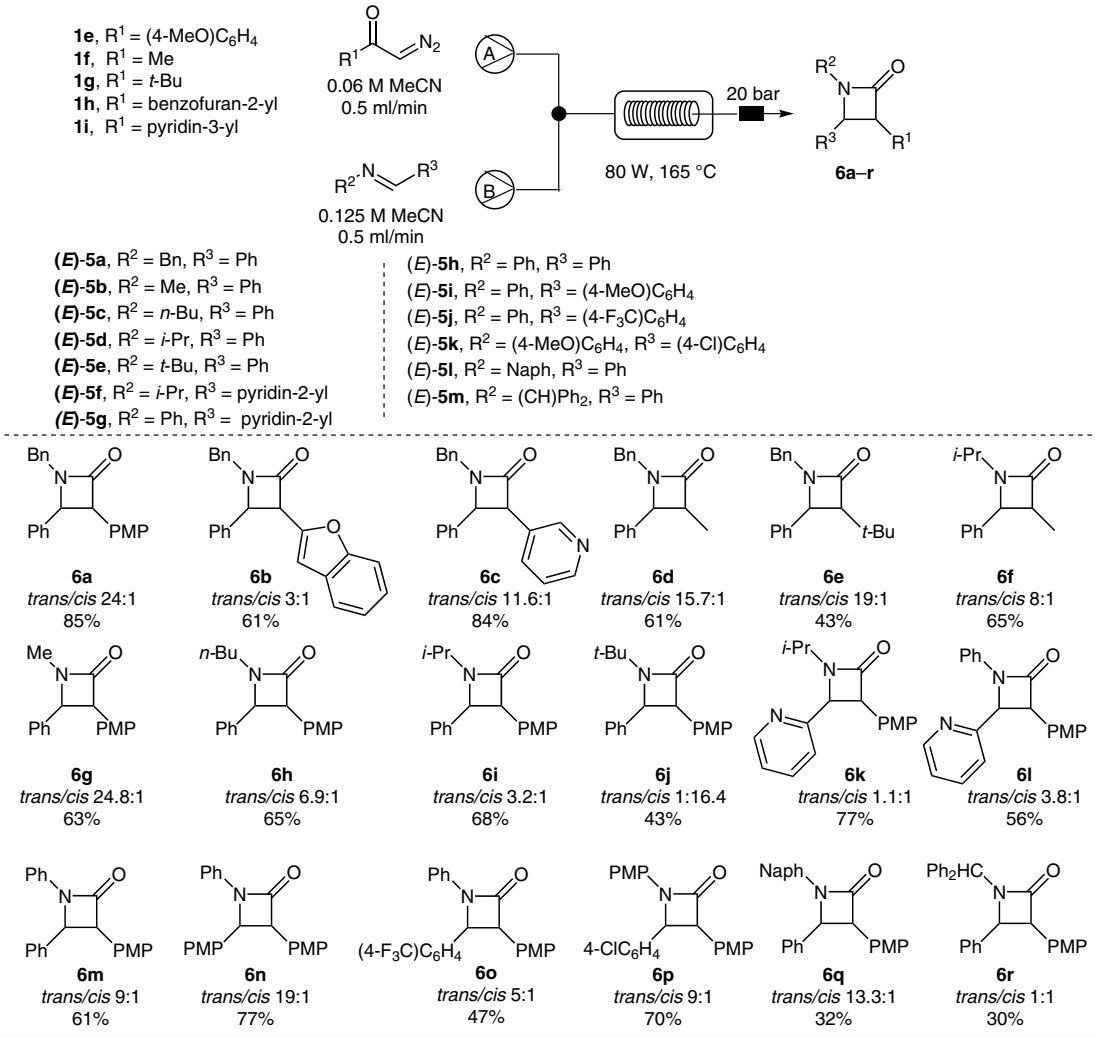

Scheme 2 Microwave-assisted Wolff–Staudinger strategy with formation of β-lactams **6a–r** *in situ* (PMP = *p*-methoxyphenyl).

confirming the crucial role of the substitution pattern of the imine in controlling the stereochemical outcome of this transformation.

These experimental results demonstrated that high diastereoselectivity in the Staudinger reaction can be achieved under high-temperature conditions for a wide range of α-diazoketones with appropriate imines. Furthermore, the high temperature reached in the flow-microwave reactor, as recorded in our experiments, appears to be a crucial parameter for the stereoselectivity of the reaction.[21]

To suggest a mechanistic model and ultimately to rationalise and predict the stereochemical outcome of the [2+2] ketene-imine cycloaddition reaction at high temperature, computational studies at the Density Functional Theory (DFT) level were performed. A number of experimental mechanistic studies[22] of the [2+2] ketene-imine cycloaddition together with DFT level calculations[23] were previously reported. Nevertheless, to our knowledge, none of the quantum chemistry calculations have been used to describe the system at high temperature. Therefore, we decided to perform a computational analysis taking into account the experimental conditions. According to the reported mechanism of this transformation,[22] the initial nucleophilic addition of imine **5** to ketene **3** would lead to the formation of a zwitterionic intermediate, **ZW**, which, in the subsequent cycloaddition step, would provide the final β-lactam **6** (Scheme 3). Firstly, the computational analysis aimed to evaluate Gibbs activation energies of the nucleophilic addition of the two isomeric imines, (*E*)-**5h** and (*Z*)-**5h** ($R^2 = R^3 = Ph$), to ketene **3e** ($R^1 = (4\text{-MeO})C_6H_4$) in *endo*- and *exo*-fashion at high temperature (165 °C). Irrespective of the imine configuration, the *exo*-addition was found to have a lower energy barrier than the *endo*-counterpart ($\Delta G_1^{\#} = 20.8$ and $\Delta G_3^{\#} = 20.4$ kcal mol^{-1} *vs.* $\Delta G_5^{\#} = 23.2$ and $\Delta G_7^{\#} = 24.3$ mol^{-1}; Scheme 3). The subsequent conrotatory ring-closure step was characterised with significantly high-

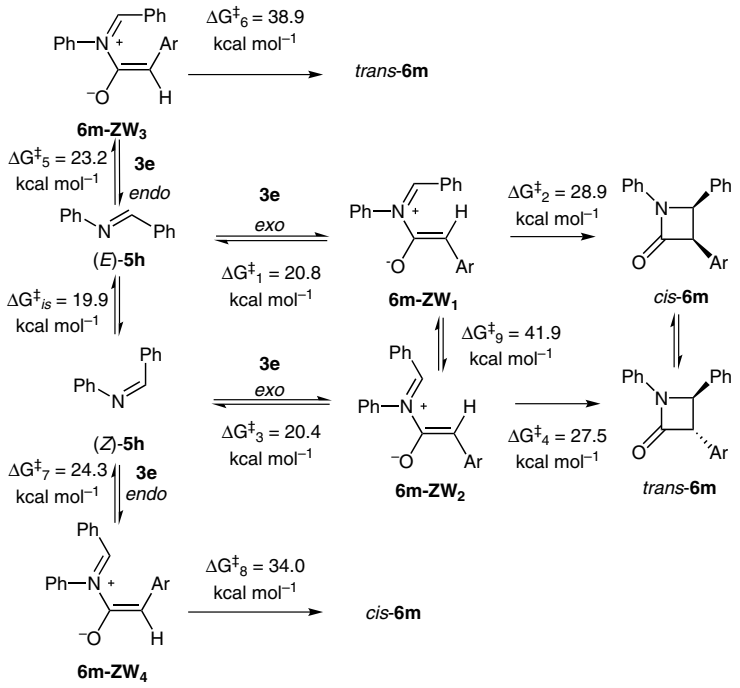

Scheme 3 Possible reaction pathways for the formation of *cis*- and *trans*-lactams **6m** by [2+2] imine-ketene cycloaddition reaction (Ar = (4-MeO)C_6H_4); the Gibbs energies shown are Gibbs energies of activation where (*E*)-**5h**+**3e** is set as the ground state; barriers $\Delta G^{\neq}_1$, $\Delta G^{\neq}_2$, $\Delta G^{\neq}_3$, $\Delta G^{\neq}_4$, $\Delta G^{\neq}_{is}$, $\Delta G^{\neq}_5$, $\Delta G^{\neq}_6$, $\Delta G^{\neq}_7$, $\Delta G^{\neq}_8$, $\Delta G^{\neq}_9$ correspond to the transition states **6m-TS$_1$**, **6m-TS$_2$**, **6m-TS$_3$**, **6m-TS$_4$**, **5h-TS**, **6m-TS$_1$-*endo***, **6m-TS$_2$-*endo***, **6m-TS$_3$-*endo***, **6m-TS$_4$-*endo***, **6m-ZW-*is***; see the Supporting Information for 3D structures).

er energy barriers for the *endo*-addition paths than for the *exo*-counterparts ($\Delta G_6^{\#}$ = 38.9 kcal mol^{-1} for **6m-ZW$_3$** and $\Delta G_8^{\#}$ = 34.0 kcal mol^{-1} for **6m-ZW$_4$** *vs.* $\Delta G_2^{\#}$ = 28.9 and $\Delta G_4^{\#}$ = 27.5 mol^{-1}, respectively, for **6m-ZW$_1$** and **6m-ZW$_2$**; Scheme 3). Based on these results, the *endo*-addition pathways were discarded from further studies for other imines. Among other possible pathways that may explain the formation of stereoisomeric lactams **6m**, the *E*/*Z* isomerisation of the zwitterionic intermediates **6m-ZW$_1$**, and **6m-ZW$_2$** was considered. This possibility was also disregarded because it would involve a rotation around the C=N bond, which would require a high energy barrier ($\Delta G_9^{\#}$ = 41.9 kcal mol^{-1}; Scheme 3). The C=N double bonds in the range of imines and zwitterionic intermediates were characterised with similar bond lengths (differences are within 1.5%; see Table 1 in the Supporting Information). This evidence suggested that they all have similar double bond character and therefore similar rotation barriers.[24]

Gibbs energies of different (*E*)- and (*Z*)-imines (**5b**, **5d**, **5e**, **5h**, **5l** and **5m** with R^3 = Ph, R^2 = Me, *i*-Pr, *t*-Bu, Ph, Naph, and (CH)Ph_2, respectively; **5f** and **5g** with R^3 = Pyridin-2-yl, R^2 = *i*-Pr and Ph, respectively), were calculated at 165 °C, finding the (*E*)-imines to be significantly more stable than their (*Z*)-counterparts for all six cases. Two alternative pathways were initially considered for the *E*/*Z* imine isomerisation: (1) through nucleophilic attack to the carbon of the iminium double bond, followed by rotation and elimination; (2) through nitrogen inversion in the starting imine. Given that the reaction was performed in acid- and metal-free conditions using anhydrous aprotic solvent (acetonitrile), the first hypothesis was not comprehensively evaluated. The second hypothetic pathway was studied deeper and the transition state **5-TS** with the linear configuration of the C=N-R moiety was characterised for the most representative cases.[25]

As expected, due to stabilisation of the linear configuration by the aromatic system,[26] the isomerisation of the imines **5h**, **5g** and **5l** were characterised with lower energy barriers ($\Delta G_{is}^{\neq}$ 19.9, 23.2 and 18.5 kcal mol^{-1}; Table 1) than other *N*-alkyl imines ($\Delta G_{is}^{\neq}$ 28.2, 28.6, 25.8, 27.9, 27.0 for **5b**, **5d**, **5e**, **5f** and **5m**, respectively; Table 1; for more details see the Supporting Information).

The possibility of the *trans*–*cis* isomerisation of the β-lactams through either retro-Staudinger cycloaddition[27] or enolisation reactions was also considered. To verify whether this side reaction occurs experimentally, a mixture of **6r** in acetonitrile (dr *trans*/*cis* 50:50) was treated under our reaction conditions (power 80 W, temperature 165 °C). The reaction mixture then was analysed by ^{1}H NMR spectroscopy, revealing that the diastereomeric ratio of the product mixture was unchanged with regard to the starting β-lactams mixture. The fact that the ratio of the two products *cis*- and *trans*-**6r** remained the same could be explained either by assuming an established thermodynamic

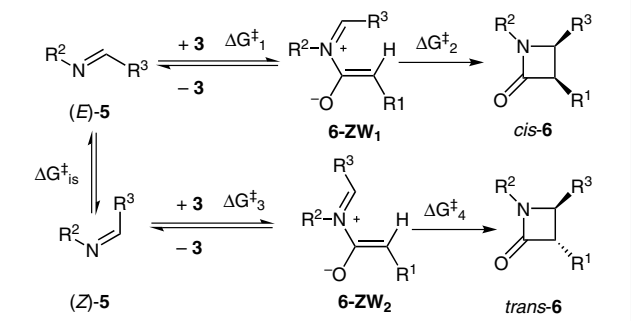

Scheme 4 Suggested operational mechanism for the formation of *cis*- and *trans*-lactams **6** by [2+2] imine–ketene cycloaddition reaction.

equilibrium between the two species, or by the absence of product interconversion. If the system was at thermodynamic equilibrium, according to the DFT calculations, the *trans*-configured product would be the prevailing component in the reaction mixture (*trans*/*cis* ratio of 3:1, calculated from ΔG_f (*trans*) = –15.8 and ΔG_f (*cis*) = –14.6 kcal mol^{-1}, respectively). This theoretical finding, contradicting the experimental result (*trans*/*cis* ratio of 1:1), could be used to rule out the *trans*/*cis* isomerisation of the lactams **6r** as a factor affecting the stereochemical outcome of the [2+2] Staudinger cycloaddition reaction. The elementary reaction steps of the [2+2] Staudinger cycloaddition[28] were computed to elucidate the operational mechanism (Scheme 4).

The steady-state approximation[29] could be applied to describe the transformations of zwitterionic intermediates **6-ZW$_1$** and **6-ZW$_2$**. The activation Gibbs energies of the key elementary steps were computed for a number of cases exhibiting different stereochemical outcome (Table 1): nucleophilic *exo*-addition of *E*/*Z* imines **5** to the ketene **3e** ($\Delta G^{\neq}_1$ and $\Delta G^{\neq}_3$ for (*E*)- and (*Z*)-imines); conrotatory ring closure of zwitterionic intermediates ($\Delta G^{\neq}_2$ and $\Delta G^{\neq}_4$ for **6-ZW$_1$** and **6-ZW$_2$**); *E*/*Z* imine **5** isomerisation ($\Delta G^{\neq}_{is}$; Table 1). These values were used to choose the mechanistic model applicable for the prediction of the diastereomeric ratios of the final products **6**. It was found that in all computed cases the conrotatory ring closure of both zwitterionic intermediates **6-ZW$_1$** and **6-ZW$_2$** was characterised with significantly higher barrier than the nucleophilic addition of the corresponding imine **5** to the ketene **3** (compare both $\Delta G^{\neq}_2$ and $\Delta G^{\neq}_4$ against $\Delta G^{\neq}_1$ and $\Delta G^{\neq}_3$, accordingly; Table 1). Moreover, the computed barrier for the ring closure of intermediate **6-ZW$_1$** derived from imine (*E*)-**5** ($\Delta G^{\neq}_2$; Table 1) was found to be either higher (Table 1, entries 1, 4, and 6–9) or similar (Table 1, entries 2, 3, and 5) to the imine (*E*)-**5** isomerisation barrier ($\Delta G^{\neq}_{is}$; Table 1). Taking into account the low concentration of ketene intermediate **3** in the reaction media, the first-order *trans*–*cis* isomerisation of imines **5** is expected to be much faster than the second-order [2+2] Staudinger reaction between isomeric imines **5** and ketene **3**. The Curtin–Hammett principle[29] could be applied and the expected *trans*/*cis* ratios of β-lactams **6** could be calculated from $\Delta\Delta G^{\#}$ of conrotatory ring closure steps. To confirm that the Curtin–Hammett principle can be successfully applied to predict *trans*/*cis* ratios for all studied cases, the diastereomeric ratios of the products **6** for the cases where imine isomerisation and the lactam ring closure had similar reaction barriers (compare $\Delta G_2^{\#}$ and $\Delta G_{is}^{\#}$ for Table 1, entries 2, 3, 5) were recalculated by using the differential rate law[30] and the activation Gibbs energy of the ketene **3e** formation from the diazocompound **1e** equal to 32.2 kcal mol^{-1} at 165 °C (see the Supporting Information for details). It was found that both approaches give the same values for *trans*/*cis* ratios, providing a good agreement with the experimental results.

Table 1 Predicted and Experimental Stereoselectivity of the [2+2] Staudinger Reaction (*T* = 165 °C)[a]

Entry	Comd	R^1	R^2	R^3	$\Delta G_{is}^{\neq}$	$\Delta G_1^{\neq}$	$\Delta G_2^{\neq}$	$\Delta G_3^{\neq}$	$\Delta G_4^{\neq}$	$\Delta\Delta G^{\neq}$[b]	*trans*/*cis* (calc.)[c]	*trans*/*cis* (exp.)[d]
1	**6f**	Me	*i*-Pr	Ph	28.6	21.1	31.8	26.4	30.0	–1.8 (–1.8)	8:1	8:1
2	**6g**	(4-MeO)C$_6$H$_4$	Me	Ph	28.2	17.3	27.7	20.0	24.3	–3.4 (–2.8)	49:1	25:1
3	**6i**	(4-MeO)C$_6$H$_4$	*i*-Pr	Ph	28.6	20.4	28.9	22.3	27.1	–1.8 (–1.0)	8:1	3:1
4	**6j**	(4-MeO)C$_6$H$_4$	*t*-Bu	Ph	25.8	21.3	28.0	25.5	30.2	+2.2 (+2.4)	1:12	1:16
5	**6k**	(4-MeO)C$_6$H$_4$	*i*-Pr	py-2-yl[e]	27.9	20.3	27.3	24.3	27.7	+0.4 (0.0)	1:2	1:1
6	**6l**	(4-MeO)C$_6$H$_4$	Ph	py-2-yl	23.2	25.2	33.2	25.2	32.7	–0.5 (–1.2)	2:1	4:1
7	**6m**	(4-MeO)C$_6$H$_4$	Ph	Ph	19.9	20.8	28.9	20.4	27.5	–1.4 (–1.9)	5:1	9:1
8	**6q**	(4-MeO)C$_6$H$_4$	Naph	Ph	18.5	22.2	31.5	21.7	28.3	–3.2 (–2.3)	40:1	13:1
9	**6r**	(4-MeO)C$_6$H$_4$	(CH)Ph$_2$	Ph	27.0	21.1	29.4	24.6	29.9	+0.5 (0.0)	1:2	1:1

[a] The Gibbs energies shown are Gibbs energies of activation (expressed in kcal mol^{-1}), where (*E*)-**5**+**3** is set as the ground state; barriers $\Delta G^{\neq}_1$, $\Delta G^{\neq}_2$, $\Delta G^{\neq}_3$, $\Delta G^{\neq}_4$, $\Delta G^{\neq}_{is}$ correspond to the transition states **6-TS$_1$**, **6-TS$_2$**, **6-TS$_3$**, **6-TS$_4$**, **5-TS**, respectively, in all computed cases; see the Supporting Information for 3D structures.
[b] Calculated by using the following formula: $\Delta\Delta G^{\#} = \Delta G_4^{\#} - \Delta G_2^{\#}$. The values derived from experimental ratios are given in brackets.
[c] Calculated at *T* = 438 K (165 °C).
[d] Determined by ^{1}H NMR spectroscopic analysis of the reaction crude mixture.
[e] Pyridin-2-yl is abbreviated py-2-yl.

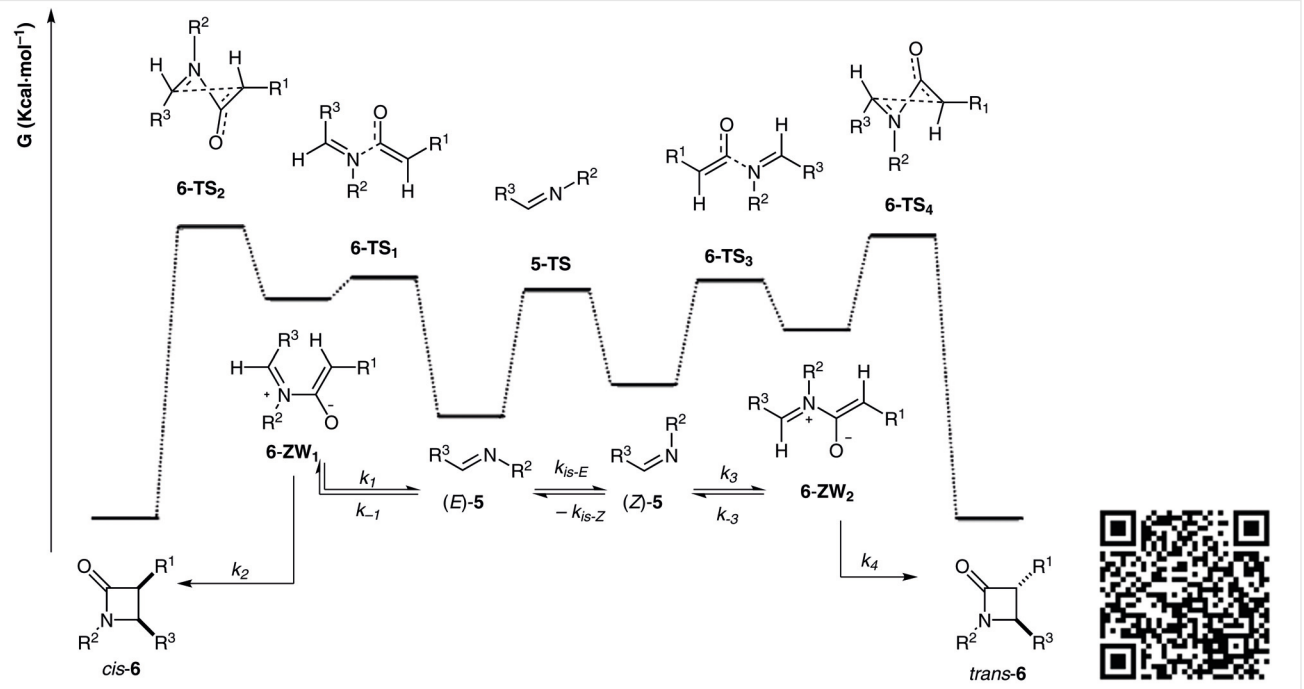

Figure 2 Reaction coordinates for the formation of *cis*- and *trans*-lactams **6** by [2+2] cycloaddition Staudinger reaction. Link to the animated 3D representation of the reaction pathways for the [2+2] Staudinger cycloaddition reactions between **5h** and **3e**, at 165 °C: https://leyscigateway.ch.cam.ac.uk/staudinger/

It can be concluded from the computational studies that the conrotatory ring closure step was the stereochemistry determining step. For a number of the computed cases, the ring closure of the zwitterion **ZW$_2$**, derived from the imine (*Z*)-**5**, was characterised by a lower barrier ($\Delta G_4^{\neq}$; Table 1) than the counterpart **ZW$_1$**, derived from the imine (*E*)-**5** ($\Delta G_2^{\neq}$; Table 1).

This could explain the *trans*-stereoselectivity observed experimentally during the [2+2] Staudinger cycloaddition reaction. However, introducing sterically large substituents (R^2) on the imine nitrogen, or electron-poor substituents (R^3) into the imine structure, diminished the difference between the rates of conrotatory closure steps of the zwitterions **ZW$_1$** and **ZW$_2$**. This resulted in deteriorated (Table 1, entries 3, 5, 6 and 9) or reversed (Table 1, entry 4) stereoselectivity of the [2+2] Staudinger reaction. In the last phase of this investigation and to facilitate the interpretation of computational data,[16] we studied the enhancement of the approach using a web-based Augmented Reality (AR) technology developed from open-source components (for technical details see the Supporting Information). Within the context of chemical applications, several AR initiatives were previously reported, mainly for educational purposes.[31] Nevertheless, to the best of our knowledge, there is no reported use of web-based AR in a chemical research program.

Our web-application allows the reader to quickly gain access to specific structural data with molecular visualisation among the large number of computed structures reported in the current account. For each computed structure the reader is directed to an HTML document by scanning a QR code or via a URL link[32] (https://leyscigateway.ch.cam.ac.uk/staudinger/viewer.html). The HTML document displays a 3D molecular representation of the structure, with the possibility for the reader to zoom, pan or rotate the 3D interactive structure, to hide the hydrogen atoms, to monitor structural parameters such as a single atom coordinates, interatomic distances, angles and dihedral angles, to export atoms coordinates as an XYZ file, or to access the 3D representation of other computed structures (Figure 3a). Finally, if the device is equipped with a camera and allows the MediaStream request,[33] the video stream is displayed on a canvas element and the reader is invited to scan a 2D fiducial marker associated with the structure. As soon as the Hamming type marker[34] is identified by the web application, it is overlaid with the 3D structure of the molecule (Figure 3b; for details see the Supporting Information). The resulting Augmented Reality experience allows the reader to quickly load, visualise and interact with multiple molecular structures simultaneously within the web interface by scanning the multiple associated 2D markers (for a maximum of 1023 different markers). Finally, our web-based viewer was also successfully employed for the semi-automatic animation of reaction path-

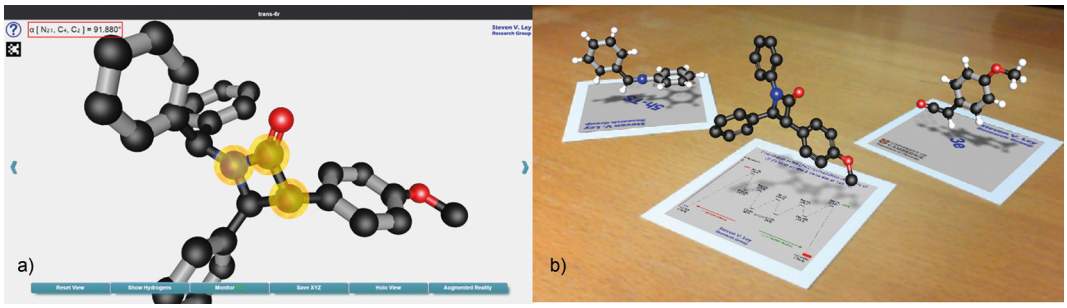

Figure 3 (a) Screen capture of the web application showing available features. (b) Screen capture of AR controls in operation.

ways by linear interpolation of each atom location between consecutive reaction points on the pathway. An application is the animated 3D representation of the reaction coordinates for the [2+2] Staudinger cycloaddition reactions between **5h** and **3e**, at 165 °C (Figure 2, for more details see the Supporting Information).

In conclusion, we have described an efficient flow route for the generation and the reaction of hazardous and reactive intermediates in a fully contained environment. The high heating efficiency of a new flow microwave reactor was applied to the preparation of primary ketenes from a range of 2-diazoketones, which were reacted in situ with amines and imines, affording amides and β-lactams, respectively. The safety and the reliability of the system during the reaction scale-up were tested, as demonstrated by the continuous multigram preparation of *N*-benzylproprionamide. The β-lactams were obtained in moderate to good yields and with a preferential *trans*-configuration. The operational mechanism of this transformation, involving a rapid isomerisation step for both aliphatic and aromatic imines at high temperature, was rationalised by DFT level calculations. The resulting computed structures were represented by means of a new web-based Augmented Reality application, which should provide wider access and dissemination of molecular computational data.

The multidisciplinary approach adopted in this work could find application in other similar synthesis programs.

Instrumentation and General Methods

Flash column chromatography (FCC) was performed using Breckland Scientific silica gel 60, particle size 40–63 nm under air pressure. Analytical thin-layer chromatography (TLC) was performed using silica gel 60 F254 pre-coated glass backed plates and visualised by ultraviolet radiation (254 nm) and/or potassium permanganate or ammonium molybdate as appropriate. Isolated yields are reported to zero decimal places and "quant." signifies a yield of 99.5% or higher. ^{1}H NMR spectra were recorded with a Bruker DRX-400 (400 MHz) or DRX-600 (600 MHz) spectrometer. Chemical shifts are reported in ppm with the resonance resulting from incomplete deuteration of the solvent as the internal standard ($CDCl_3$: δ = 7.26 ppm). ^{13}C NMR spectra were recorded with a Bruker DRX-400 (100 MHz) or DRX-600 (150 MHz) spectrometer with complete proton decoupling. Chemical shifts are reported in ppm with the solvent resonance as the internal standard ($CDCl_3$: δ = 77.0 ppm). Data are reported as follows: chemical shift δ/ppm, multiplicity (s = singlet, d = doublet, t = triplet, q = quartet, br = broad, m = multiplet or combinations thereof; ^{13}C signals are singlets unless otherwise stated), coupling constants are reported in Hz, integration (^{1}H only). ^{1}H NMR signals are reported to two decimal places and ^{13}C signals to one decimal place unless rounding would produce a value identical to another signal; in this case, an additional decimal place is reported for both signals concerned. ^{19}F NMR signals are reported to two decimal places and trifluorotoluene was used as internal standard (δ = –63.72 ppm). High-resolution mass spectrometry (HRMS) was performed with a Waters Micromass LCT spectrometer using electrospray ionisation, time-of-flight analysis and Micromass MS software HRMS signals are reported to four decimal places and are within ±5 ppm of theoretical values. IR spectra were recorded neat as thin films with a Perkin–Elmer Spectrum One FTIR spectrometer; only selected peaks are reported. Melting points were collected with a Stanford Research Systems Optimelt automated melting point system using a gradient of 1 °C per min. Unless stated otherwise, reagents were obtained from commercial sources and used without purification. The removal of solvent under reduced pressure was carried out with a standard rotary evaporator.

Geometries of all structures (minima and saddle points) were optimised at the ωB97xd/cc-PVDZ level ωB97xD/cc-PVTZ//ωB97xD/cc-PVDZ[35] level calculations[36] using the implicit Solvation Model based on Density (SMD)[37] implemented in Gaussian 09 software[38] in acetonitrile as a solvent (using the SMD solvation model, ε = 35.688). Subsequent vibrational frequency calculations were performed at the same level for all calculated structures. When needed, multiple initial guesses (no more than four) were used to explore the conformational space fully. All transition states thus found possess exactly one negative Hessian eigenvalue, while all other stationary points were confirmed to be genuine minima on the potential energy surface (PES). Intrinsic reaction coordinate (IRC) analysis was performed to unambiguously assign located transition states when needed. Electronic energies were obtained by performing single-point calculations at the ωB97xd/cc-pVTZ level in solvent. Gibbs energies were calculated as $\Delta G = \Delta H - T\Delta S$ at 438 K where enthalpies and entropies were obtained by using standard statistical mechanical formulae for the ideal gas, rigid rotor, and harmonic oscillator approximations following the normal-mode analysis in vacuum. A correction of $(3.0 \cdot \Delta n)$ kcal mol^{-1} (corresponding to the difference between the concentration of the ideal gas at 438 K and 1 atm and its 1 mol l^{-1} concentration; Δn is the change in number of moles in the reaction) has been applied so that the computed values refer to 1 mol l^{-1} standard state at a given temperature.

For each computed structure a JavaScript file was generated. This file consisted of an array of atoms describing the element and Cartesian coordinates for each atom and an array of bonds with their computed multiplicity. The JavaScript file was passed to a client-side HTML viewer where each atom object was constructed from a JavaScript atom object prototype, defining atomic radius[39] and CPK colouring[40] for each element. Each atom object was then rendered as an icosahedral geometric primitive at its location with the required radius and colour, using the WebGL API through the open-source three.js library.[41] For each interatomic bond, two half-bond objects were generated. The two half-bond objects were parented with the atom object they respectively originate from before being rendered as two collinear cylindrical geometric primitives. For each half-bond geometry, the direction was set parallel to the interatomic bond orientation, while the length was constrained to the half value of the interatomic distance. Both length and direction of the half-bond could be constrained for each frame, allowing the animation of the molecular structure by only interpolation of the atoms position. The amount as well as the radius of cylindrical geometries for a single interatomic bond was defined by the computed multiplicity of the bond. For multiple bonds, cylindrical geometries were distributed on the plane defined by the positions of three geminal atoms. Considering the relatively low molecular weight of most of the computed structures, the 3D molecular representation of each molecule could be quickly achieved with a minimal amount of geometric primitives and without the need for the implementation of geometry shaders (i.e., ray-casted geometry impostors) in WebGL1.0 in order to save on graphic rendering resources.[42] However, as the simultaneous representation of several computed structures within the same WebGL renderer was required, each molecular structure was exported as a JSON file[43] to be called on request. The molecular structures were rendered in a standard three.js scene.[44] For the Augmented Reality, the camera calibration, adaptive thresholding, contours detection, corners sorting, markers identification and coplanar pose estimation were handled by the OpenCV.js and js-ArUco.js libraries.[45] The resulting computed extrinsic parameters of the camera were then employed to overlay the molecular structures to their associated marker, with the help of a modified version of the skarf.js library,[46] developed by our group. A simple performance test was carried out by tracking several ArUco markers simultaneously on a 640 × 480 pixel canvas HTML element, on a standard desktop PC (Dell™ Optiplex9010, 3.4 GHz Intel® Core™ i7–3770 CPU, 8 GB of RAM, Windows7™ – 64 bits) equipped with a web camera (Microsoft® LifeCam Cinema™, wide angle F/2.0 HD lens, 720p HD 30 fps, Autofocus) and running Mozilla Firefox™ 44.0 or Google Chrome™ 48 (for more details see Figure 4).

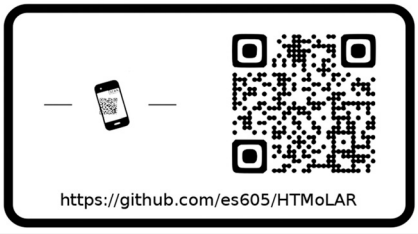

Figure 4 Link to the web-based interactive 3D molecular viewer with AR. https://github.com/es605/HTMoLar

Preparation of 2-Diazoketones 1a–l; General Procedure

Compounds **1a–e** and **1h–i** were prepared according to a reported procedure by reaction of bromoacetates with *N*,*N*′-ditosylhydrazine and DBU.[47] Compounds **1f** and **1g** were prepared according to a reported two-step procedure by reaction of acetylketones with 4-acetamidobenzenesulfonylazide (*p*-ABSA),[48] and subsequent basic treatment (NaOH 1 M) of the resulting diazo-diketone derivatives.[49] The spectroscopic data of **1f**[48] and **1g**[50] are in accordance with reported values.

2-Diazo-1-[4-(trifluoromethyl)phenyl]-ethan-1-one (1a)

Yield: 52%; yellow solid; mp 64–65 °C.

^{1}H NMR (400 MHz, $CDCl_3$): δ = 7.86 (d, *J* = 8.1 Hz, 2 H), 7.71 (d, *J* = 8.2 Hz, 2 H), 5.94 (s, 1 H).

^{13}C NMR (150.0 MHz, $CDCl_3$): δ = 184.9, 139.4, 134.1 (q, *J* = 32.7 Hz), 127.1, 125.7 (q, *J* = 3.7 Hz), 123.5 (q, *J* = 272.3 Hz), 55.0.

^{19}F NMR (100.0 MHz, $CDCl_3$): δ = 64.0.

IR (neat): 3084, 2106, 1600, 1415, 1319, 1111, 860 cm^{-1}.

Anal. Calcd. for $C_9H_5F_3N_2O$: C, 50.48; H, 2.35; N, 13.08. Found: C, 50.88; H, 2.30; N, 12.60.

Preparation of Amides 4a–f; General Procedure

A solution of 2-diazoketone **1e–f** (0.06 M in MeCN) and benzylamine **2** (0.12 M in MeCN) were pumped into the tubular glass reactor covered with a polytetrafluoroethylene film for safety and insulation reasons (i.d. 3.6 mm, internal volume: 5.5–6.0 mL) at the same flow rate (total flow rate of 1.0 mL min^{-1}). An internal pressure of 2.0 MPa by a back pressure regulator (BPR) and a MW irradiation of 80 W were assured. After 10 min, the exit temperature reached a steady state at 165 °C (Figure 1d; green line), and collection of the crude reaction mixture was started at this time. The crude product was concentrated *in vacuo* and the residue was purified by flash column chromatography on silica gel (hexane–EtOAc) to give amides **4a–f**. CAUTION: special precautions must be taken because of the hazards associated with diazo compounds and the ketene derivatives. All work was carried in a well ventilated fumehood, with an automatic shut down of the system in case of an increase of the temperature and pressure over the maximum value set. The spectroscopic data of **4b**,[51] **4c**,[52] **4d**,[53] **4e**,[54] and **4f**[50] are in accordance with reported values.

N-Benzyl-2-[4-(trifluoromethyl)phenyl]acetamide (4a)

Yield: 65%; white solid; mp 134–136 °C.

^{1}H NMR (600 MHz, $CDCl_3$): δ = 7.61 (d, *J* = 8.05 Hz, 2 H), 7.41 (d, *J* = 8.00 Hz, 2 H), 7.32 (d, *J* = 7.53 Hz, 2 H), 7.28–7.34 (m overlapping d at 7.32 ppm, 1 H), 7.22 (d, *J* = 7.13 Hz, 2 H), 5.89 (br. s, 1 H), 4.43 (d, *J* = 5.8 Hz, 2 H), 3.64 (s, 2 H).

^{13}C NMR (150.0 MHz, $CDCl_3$): δ = 169.7, 138.8 (br s), 137.8, 129.6, 129.59 (q, J_{C-F} = 32.5 Hz), 128.7, 127.62, 127.59, 125.8 (q, J_{C-F} = 3.8 Hz), 124.0 (q, J_{C-F} = 272.0 Hz), 43.8, 43.3.

IR (neat): 3238, 3063, 1625, 1556, 1328, 1122, 1070, 753, 698 cm^{-1}.

HRMS: *m*/*z* [M + H]$^+$ calcd for $C_{15}H_{15}F_3NO$: 294.1100; found: 294.1090.

Preparation of Imines (*E*)-5a–m; General Procedure

Imines (*E*)-**5a** and (*E*)-**5b** were obtained from commercial sources and used without purification. All the other imines were prepared according a reported procedure by reaction of appropriate aldehyde and

imine in dichloromethane in the presence of $MgSO_4$.[55] The spectroscopic data of (*E*)-**5c–e**,[56] (*E*)-**5h–j**,[57] (*E*)-**5f**,[58] (*E*)-**5g**,[59] (*E*)-**5k**,[60] (*E*)-**5l**,[61] and (*E*)-**5m**[47] are in accordance with reported values.

Preparation of β-Lactams 6a–r; General Procedure

A solution of 2-diazoketone **1e–i** (0.06 M in MeCN) and the appropriate imine **5a–m** (0.125 M in MeCN) were pumped into the tubular glass reactor covered with a polytetrafluoroethylene film for safety and insulation reasons (i.d. 3.6 mm, internal volume: 5.5–6.0 mL) at the same flow rate (total flow rate of 1.0 mL min^{-1}). An internal pressure of 2.0 MPa by a back pressure regulator (BPR) and a MW irradiation of 80 W were assured. After 10 min, the exit temperature reached a steady state at 165 °C (Figure 1d; green line), and collection of the crude reaction mixture was started at this time. The crude product was concentrated *in vacuo*, and the residue was purified by flash column chromatography on silica gel (hexane–EtOAc) to give β-lactams **6a–r**. CAUTION: special precautions must be taken because of the hazards associated with the diazo compounds and the ketene derivatives. All work was carried in a well ventilated fumehood, with an automatic shut down of the system in case of an increase of the temperature and pressure over the maximum value set. The spectroscopic data of *trans*-**6a**,[62] *trans*-**6d**,[20] *trans*-**6g**,[63] *trans*-**6i**,[55] *cis*-**6j**,[64] *trans*-**6m**,[55] and *trans*-**6n**,[65] are in accordance with reported values.

1-Benzyl-3-(benzofuran-2-yl)-4-phenylazetidin-2-one (*trans*-6b)

Yield: 61%; yellow oil; dr *trans*/*cis* 92:8.

^{1}H NMR (600 MHz, $CDCl_3$): δ = 7.52 (d, *J* = 7.6 Hz, 1 H), 7.24–7.46 (m, 12 H), 7.21 (td, *J* = 7.5, 1.0 Hz, 1 H), 6.64 (s, 1 H), 5.00 (d, *J* = 15.1 Hz, 1 H), 4.64 (d, *J* = 2.4 Hz, 1 H), 4.38 (d, *J* = 2.3 Hz, 1 H), 3.92 (d, *J* = 15.2 Hz, 1 H).

^{13}C NMR (150.0 MHz, $CDCl_3$): δ = 165.5, 155.0, 150.7, 136.6, 135.1, 129.1, 128.9, 128.8, 128.4, 128.2, 127.8, 126.5, 124.3, 122.9, 120.9, 111.1, 105.2, 60.4, 59.1, 44.9.

IR (neat): 3674, 2988, 1755, 1453, 1252, 1076, 725 cm^{-1}.

HRMS: *m*/*z* $[M + H]^+$ calcd for $C_{24}H_{20}NO_2$: 354.1494; found: 354.1503.

Additional data related to this publication are available at the http://dx.doi.org/10.17863/CAM.654 data repository.

Acknowledgment

The authors would like to acknowledge Dr Aki Tomita and Professor Jonathan M. Goodman for helpful discussions and suggestions. The authors are also thankful to the EPSRC (Award Nos. EP/K009494/1, EP/K039520/1 and EP/M004120/1) for financial support.

Supporting Information

Supporting information for this article is available online at http://dx.doi.org/10.1055/s-0035-1562579.

References

(1) Hessel, V.; Kralisch, D.; Kockmann, N. In *Novel Process Windows: Innovative Gates to Intensified and Sustainable Chemical Processes*, 1st Ed.; Wiley-VCH Verlag: Weinheim, **2015**.

(2) (a) Mitic, A.; Gernaey, K. V. *Chem. Eng. Technol.* **2015**, *38*, 1699. (b) Hessel, V.; Kralisch, D.; Kockmann, N.; Noël, T.; Wang, Q. *ChemSusChem* **2013**, *6*, 746. (c) Ley, S. V. *Chem. Rec.* **2012**, *12*, 378. (d) McQuade, D. T.; Seeberger, P. H. *J. Org. Chem.* **2013**, *78*, 6384.

(3) (a) Porta, R.; Benaglia, M.; Puglisi, A. *Org. Process Res. Dev.* **2016**, *20*, 2. (b) Baumann, M.; Baxendale, I. R. *Beilstein J. Org. Chem.* **2015**, *11*, 1194. (c) Ghislieri, D.; Gilmore, K.; Seeberger, P. H. *Angew. Chem. Int. Ed.* **2014**, 678. (d) Gutmann, B.; Cantillo, D.; Kappe, C. O. *Angew. Chem. Int. Ed.* **2015**, *54*, 6688.

(4) (a) Ley, S. V.; Fitzpatrick, D. E.; Ingham, R. J.; Myers, R. M. *Angew. Chem. Int. Ed.* **2015**, *54*, 3449. (b) Ley, S. V.; Fitzpatrick, D. E.; Myers, R. M.; Battilocchio, C.; Ingham, R. J. *Angew. Chem. Int. Ed.* **2015**, *54*, 10122.

(5) (a) Kirschning, A.; Solodenko, W.; Mennecke, K. *Chem. Eur. J.* **2006**, *12*, 5972. (b) Tsubogo, T.; Oyamada, H.; Kobayashi, S. *Nature* **2015**, *520*, 329. (c) Munirathinam, R.; Huskens, J.; Verboom, W. *Adv. Synth. Catal.* **2015**, *357*, 1093. (d) Hornung, C.; Hallmark, B.; Mackley, M. R.; Baxendale, I. R.; Ley, S. V. *Adv. Synth. Catal.* **2010**, *352*, 1736. (e) Suzuki, Y.; Laurino, P.; McQuade, D. T.; Seeberger, P. H. *Helv. Chim. Acta* **2012**, *95*, 2578. (f) Brahma, A.; Musio, B.; Ismayilova, U.; Nikbin, N.; Kamptmann, S. B.; Siegert, P.; Jeromin, G.; Ley, S. V.; Pohl, M. *Synlett* **2015**, 262.

(6) (a) Gilmore, K.; Seeberger, P. H. *Chem. Rec.* **2014**, *14*, 410. (b) Baumann, M.; Baxendale, I. R. *React. Chem. Eng.* **2016**, 11. (c) Plutschack, M. B.; Correia, C. A.; Seeberger, P. H.; Gilmore, K. *Organic Photoredox Chemistry in Flow*, In *Top. Organomet. Chem.*; vol. 27; Noël, T., Ed.; Springer: Switzerland, **2015**, 43–76. (d) Schuster, E. M.; Wipf, P. *Isr. J. Chem.* **2014**, *54*, 361. (e) Su, Y.; Straathof, N. J. W.; Hessel, V.; Noël, T. *Chem. Eur. J.* **2014**, *20*, 10562. (f) Garlets, Z. J.; Nguyen, J. D.; Stephenson, C. R. J. *Isr. J. Chem.* **2014**, *54*, 351.

(7) (a) Roth, G. P.; Stalder, R.; Long, T. R.; Sauer, D. R.; Djuric, S. W. *J. Flow Chem.* **2013**, *3*, 34. (b) Kabeshov, M.; Musio, B.; Murray, P. R. D.; Browne, D. L.; Ley, S. V. *Org. Lett.* **2014**, *16*, 4618. (c) Stalder, R.; Roth, G. P. *ACS Med. Chem. Lett.* **2013**, *4*, 1119. (d) Watts, K.; Gattrell, W.; Wirth, T. *Beilstein J. Org. Chem.* **2011**, *7*, 1108.

(8) (a) Cintas, P.; Tagliapietra, S.; Caporaso, M.; Tabasso, S.; Cravotto, G. *Ultrason. Sonochem.* **2015**, *25*, 8. (b) Brasholz, M.; Johnson, B.; Macdonald, J. M.; Polyzos, A.; Tsanaktsidis, J.; Saubern, S.; Holmes, A. B.; Ryan, J. H. *Tetrahedron* **2010**, *66*, 6445.

(9) (a) Kappe, C. O. *Angew. Chem. Int. Ed.* **2004**, *43*, 6250. (b) Gawande, M. B.; Shelke, S. N.; Zboril, R.; Varma, R. S. *Acc. Chem. Res.* **2014**, *47*, 1338. (c) Dudley, G. B.; Stiegman, A. E. *Chem. Sci.* **2015**, *6*, 2144.

(10) (a) Kappe, C. O.; Pieber, B.; Dallinger, D. *Angew. Chem. Int. Ed.* **2013**, *52*, 1088. (b) Glasnov, T. N.; Kappe, C. O. *Chem. Eur. J.* **2011**, *17*, 11956. (c) Xolin, A.; Stévenin, A.; Pucheault, M.; Norsikian, S.; Boyer, F.-D.; Beau, J.-M. *Org. Chem. Front.* **2014**, *1*, 992. (d) Damm, M.; Glasnov, N. T.; Kappe, C. O. *Org. Process Res. Dev.* **2010**, *14*, 215. (e) Kunz, U.; Turek, T. *Beilstein J. Org. Chem.* **2009**, *5*, 1. (f) Ceylan, S.; Coutable, L.; Wegner, J.; Kirschning, A. *Chem. Eur. J.* **2011**, *17*, 1884. (g) Kirschning, A.; Kupracz, L.; Hartwig, J. *Chem. Lett.* **2012**, *41*, 562.

(11) (a) Smith, C. J.; Iglesias-Sigüenza, F. J.; Baxendale, I. R.; Ley, S. V. *Org. Biomol. Chem.* **2007**, *5*, 2758. (b) Baxendale, I. R.; Hayward, J. J.; Ley, S. V. *Comb. Chem. High Throughput Screening* **2007**, *35*, 802. (c) Glasnov, T. N.; Kappe, C. O. *Macromol. Rapid Commun.* **2007**, *28*, 395. (d) Singh, B. K.; Kaval, N.; Tomar, S.; Van Der Eycken, E.; Parmar, V. S. *Org. Process Res. Dev.* **2008**, *12*, 468.

(e) Baxendale, I. R.; Hornung, C.; Ley, S. V.; Molina, J. de M. M.; Wikström, A. *Aust. J. Chem.* **2013**, *66*, 131. (f) Bagley, M. C.; Jenkins, R. L.; Lubinu, M. C.; Mason, C.; Wood, R. *J. Org. Chem.* **2005**, *70*, 7003.

(12) De La Hoz, A.; Alcázar, J.; Carillo, J.; Herrero, M. A.; Muñoz, J. D. M.; Prieto, P.; De Cózar, A.; Diaz-Ortiz, A. *Reproducibility and Scalability of Microwave-Assisted Reactions*, In *Microwave Heating*; Chandra, U., Ed.; InTech: Rijeka, Croatia, **2011**, pp 137–162; available at www.intechopen.co.

(13) (a) Strauss, C. R. *Chem. Aust.* **1990**, 186. (b) Chen, S.-T.; Chiou, S.-H.; Wang, K.-T. *J. Chem. Soc., Chem. Commun.* **1990**, 807.

(14) (a) Sauks, J. M.; Mallik, D.; Lawryshyn, Y.; Bender, T.; Organ, M. *Org. Process Res. Dev.* **2014**, *18*, 1310. (b) Patil, N. G.; Benaskar, F.; Rebrov, E. V.; Meuldijk, J.; Hulshof, L. A.; Hessel, V.; Schouten, J. C. *Org. Process Res. Dev.* **2014**, *18*, 1400. (c) Horikoshi, S.; Sumi, T.; Serpone, N. *Chem. Eng. Process.: Process Intensif.* **2013**, *73*, 59.

(15) (a) Wolff, L. *Justus Liebigs Ann. Chem.* **1902**, *325*, 129. (b) Meier, B. H. *Angew. Chem. Int. Ed. Engl.* **1975**, *14*, 32.

(16) Yokozawa, S.; Ohneda, N.; Muramatsu, K.; Okamoto, T.; Odajima, H.; Ikawa, T.; Sugiyama, J.; Fujita, M.; Sawairi, T.; Egami, H.; Hamashima, Y.; Egi, M.; Akai, S. *RSC Adv.* **2015**, *5*, 10204.

(17) Morschhäuser, R.; Krull, M.; Kayser, C.; Boberski, C.; Bierbaum, R.; Püschner, P. A.; Glasnov, T. N.; Kappe, C. O. *Green Process. Synth.* **2012**, *1*, 281.

(18) (a) Kappe, C. O. *Chem. Soc. Rev.* **2013**, *42*, 4977. (b) Hartwig, J.; Kirschning, A. *Chem. Eur. J.* **2016**, *22*, 3044.

(19) Tenud, L. *Helv. Chim. Acta* **1977**, *60*, 975.

(20) Hafner, A.; Ley, S. V. *Synlett* **2015**, *26*, 1470.

(21) (a) Linder, M. R.; Podlech, J. *Org. Lett.* **2001**, *3*, 1849. (b) Bandyopadhyay, D.; Banik, B. K. *Helv. Chim. Acta* **2010**, *93*, 298. (c) Prieto, P.; Liu, R. *Org. Biomol. Chem.* **2010**, *8*, 929.

(22) (a) Qi, H.; Li, Z.; Xu, J. *Org. Biomol. Chem.* **2011**, *9*, 2702. (b) Li, B.; Wang, Y.; Du, D.-M.; Xu, J. *J. Org. Chem.* **2007**, *72*, 990. (c) Jiao, L.; Liang, Y.; Xu, J. *J. Am. Chem. Soc.* **2006**, *128*, 6060. (d) Liang, Y.; Jiao, L.; Zhang, S.; Xu, J. *J. Org. Chem.* **2005**, *70*, 334. (e) Yang, Z.; Xu, J. *Tetrahedron Lett.* **2012**, *53*, 786.

(23) (a) Domingo, L. R.; Rios-Gutierrez, M.; Saez, J. A. *RSC Adv.* **2015**, *5*, 37119. (b) Cossio, F. P.; Arrieta, A.; Sierra, M. A. *Acc. Chem. Res.* **2008**, *41*, 925. (c) Banik, B. K.; Lecea, B.; Arrieta, A.; de Cozar, A.; Cossio, F. P. *Angew. Chem. Int. Ed.* **2007**, *46*, 3028. (d) Arrieta, A.; Lecea, B.; Cossio, F. P. *Top. Heterocycl. Chem.* **2010**, *22*, 313.

(24) Pauling, L. *Orv. Hetil.* **1969**, *110*, 549.

(25) Blanco, F.; Alkorta, I.; Elguero, J. *Croat. Chem. Acta* **2009**, *82*, 173.

(26) *Endo*-addition pathways have been also analysed for *N*-methyl and *N*-*tert*-butylbenzylideneimines **4b** and **4e**. Similar to the described *N*-phenylbenzylideneimine **4h**, they were characterised with higher activation barriers. For the 3D structures, see the Supporting Information

(27) Wright, S. W. In *Name Reactions for Carbocyclic Ring Formations*; Li, J. J., Ed.; John Wiley & Sons: Hoboken, NJ, **2010**, pp 45–69.

(28) Kirmse, W.; Rondan, N. G.; Houk, K. N. *J. Am. Chem. Soc.* **1984**, *106*, 7989.

(29) IUPAC, *Compendium of Chemical Terminology, 2nd ed. (the "Gold Book")*; Compiled, by. McNaught A. D.; Wilkinson, A., Eds.; Blackwell Scientific Publications: Oxford, **1997**, XML online corrected version: http://goldbook.iupac.org (2006) created by Nic M., Jirat J., Kosata B., updates compiled by A. Jenkins. ISBN 0-9678550-9-8.

(30) Harvey, M. J.; Mason, N. J.; Rzepa, H. S. *J. Chem. Inf. Model.* **2014**, *54*, 2627.

(31) (a) Gillet, A.; Sanner, M.; Stoffler, D.; Goodsell, D.; Olson, A. *IEEE Visualization* **2004**, 235. (b) Nunez, M.; Quiros, R.; Nunez, I.; Carda, J. B.; Camahort, E. *5th WSEAS / IASME (EE'08)* **2008**, 271–277. (c) http://elements4d.daqri.com/#lessons. (d) http://sponholtzproductions.com/Product_Reviews.html.

(32) Acronyms: Quick Response (QR) and Uniform Resource Locator (URL).

(33) https://developer.mozilla.org/en/docs/Web/API/MediaStream.

(34) Hamming, R. W. *Bell Syst. Tech. J.* **1950**, *29*, 147.

(35) (a) Chai, J.-D.; Head-Gordon, M. *Phys. Chem. Chem. Phys.* **2008**, *10*, 6615. (b) Kendall, R. A.; Dunning, T. H. Jr.; Harrison, R. J. *J. Chem. Phys.* **1992**, *96*, 6796.

(36) For benchmarking studies showing high accuracy and applicability of the ωB97xD/cc-PVTZ//ωB97xD/cc-PVDZ method to organic transformations, see: (a) Schenker, S.; Schneider, C.; Tsogoeva, S. B.; Clark, T. *J. Chem. Theory Comput.* **2011**, *7*, 3586. (b) Kabeshov, M. A.; Kysilka, O.; Rulíšek, L.; Suleimanov, Y. V.; Bella, M.; Malkov, A. V.; Kočovský, P. *Chem. Eur. J.* **2015**, *21*, 12026.

(37) Acetonitrile (ε = 35.688) was used as solvent; for more details see: Marenich, A. V. Cramer C. J.; Truhlar, D. G. *J. Phys. Chem. B* **2009**, *113*, 6378.

(38) *Gaussian 09, Revision D.01*; Frisch, M. J.; Trucks, G. W.; Schlegel, H. B.; Scuseria, G. E.; Robb, M. A.; Cheeseman, J. R.; Scalmani, G.; Barone, V.; Mennucci, B.; Petersson, G. A.; Nakatsuji, H.; Caricato, M.; Li, X.; Hratchian, H. P.; Izmaylov, A. F.; Bloino, J.; Zheng, G.; Sonnenberg, J. L.; Hada, M.; Ehara, M.; Toyota, K.; Fukuda, R.; Hasegawa, J.; Ishida, M.; Nakajima, T.; Honda, Y.; Kitao, O.; Nakai, H.; Vreven, T.; Montgomery, J. A. Jr.; Peralta, J. E.; Ogliaro, F.; Bearpark, M.; Heyd, J. J.; Brothers, E.; Kudin, K. N.; Staroverov, V. N.; Kobayashi, R.; Normand, J.; Raghavachari, K.; Rendell, A.; Burant, J. C.; Iyengar, S. S.; Tomasi, J.; Cossi, M.; Rega, N.; Millam, M. J.; Klene, M.; Knox, J. E.; Cross, J. B.; Bakken, V.; Adamo, C.; Jaramillo, J.; Gomperts, R.; Stratmann, R. E.; Yazyev, O.; Austin, A. J.; Cammi, R.; Pomelli, C.; Ochterski, J. W.; Martin, R. L.; Morokuma, K.; Zakrzewski, V. G.; Voth, G. A.; Salvador, P.; Dannenberg, J. J.; Dapprich, S.; Daniels, A. D.; Farkas, Ö.; Foresman, J. B.; Ortiz, J. V.; Cioslowski, J.; Fox, D. J., Eds.; Gaussian, Inc.: Wallingford CT, **2013**.

(39) The SMD intrinsic atomic Coulomb radii were used as implemented in NWChem software.

(40) http://www.nwchem-sw.org/index.php/Release65:SMD_Model.

(41) http://en.wikipedia.org/wiki/CPK_coloring.

(42) (a) Tarini, M.; Cignoni, P.; Montani, C. *IEEE Trans. Vis. Comput. Graph.* **2006**, *12*, 1237. (b) Rose, A. S.; Hildebrand, P. W. *Nucleic Acids Res.* **2015**, *1*, 1; for more details, see: http://proteinformatics.charite.de/ngl/html/ngl.html. (c) Rego, N.; Koes, D. *Bioinformatics* **2014**, *8*, 1322; for more details, see: http://3dmol.csb.pitt.edu/index.html. (d) Mwalongo, F.; Krone, M.; Becher, M.; Reina, G.; Ertl, T. In *Proceeding Web3D '15. Proceeding of the 20th international conference on 3D web technology*; pp. 115–122.

(43) https://developer.mozilla.org/en/docs/Web/JavaScript/Reference/Global_Objects/JSON.

(44) Revision 73. For more details, see: http://threejs.org/.

(45) (a) Garrido-Jurado, S.; Muñoz-Salinas, R.; Madrid-Cuevas, F. J.; Marín-Jiménez, M. J. *Pattern Recognition* **2014**, *47*, 2280; https://github.com/jcmellado/js-aruco. (b) http://opencv.org/

(46) http://cg.skeelogy.com/skarfjs/.

(47) Toma, T.; Shimokawa, J.; Fukuyama, T. *Org. Lett.* **2007**, *9*, 10.

(48) Sharpe, R. J.; Malinowski, J. T. Johnson J. S. *J. Am. Chem. Soc.* **2013**, *135*, 17990.

(49) Lancou, A.; Haroun, H.; Kundu, U. K.; Legros, F.; Zimmermann, N.; Mathe-Allainmat, M.; Lebreton, J.; Dujardin, G.; Gaulon-Nourry, C.; Gosselin, P. *Tetrahedron* **2012**, *68*, 9652.
(50) Nikolaev, V. A.; Utkin, P. Y.; Korobitsyna, I. K. *Zh. Org. Khim.* **1989**, *25*, 1176.
(51) Watson, A. J. A.; Wakeham, R. J.; Maxwell, A. C.; Williams, J. M. J. *Tetrahedron* **2014**, *70*, 3683.
(52) Lundberg, H.; Tinnis, F.; Adolfsson, H. *Synlett* **2012**, *23*, 2201.
(53) Starkov, P.; Sheppard, T. D. *Org. Biomol. Chem.* **2011**, *9*, 1320.
(54) Ghosh, S. C.; Hong, S. H. *Eur. J. Org. Chem.* **2010**, 4266.
(55) Ramalingam, B.; Seayad, A. M.; Chuanzhao, L.; Garland, M.; Yoshinaga, K.; Wadamoto, M.; Nagata, T.; Chai, C. L. L. *Adv. Synth. Catal.* **2010**, *352*, 2153.
(56) Perrone, S.; Salomone, A.; Caroli, A.; Falcicchio, A.; Citti, C.; Cannazza, G.; Troisi, L. *Eur. J. Org. Chem.* **2014**, 5932.
(57) Shu, W. M.; Ma, J. R.; Zheng, K. L.; Sun, H. Y.; Wang, M.; Yang, Y.; Wu, A. X. *Tetrahedron* **2014**, *70*, 9321.
(58) Schoumacker, S.; Hamelin, O.; Téti, S.; Pécaut, J.; Fontecave, M. *J. Org. Chem.* **2005**, *70*, 301.
(59) Troisi, L.; Ronzini, L.; Granito, C.; Vitis, L. D.; Pindinelli, E. *Tetrahedron* **2006**, *62*, 1564.
(60) Bennett, J. S.; Charles, K. L.; Miner, M. R.; Heuberger, C. F.; Spina, E. J.; Bartels, M. F.; Foreman, T. *Green Chem.* **2009**, *11*, 166.
(61) Knöpke, L. R.; Nemati, N.; Köckritz, A.; Brückner, A.; Bentrup, U. *ChemCatChem* **2010**, *2*, 273.
(62) Kim, I.; Roh, S. W.; Lee, D. G.; Lee, C. *Org. Lett.* **2014**, *16*, 2482.
(63) Zhang, Z.; Liu, Y.; Ling, L.; Li, Y.; Dong, Y.; Gong, M.; Zhao, X.; Zhang, Y.; Wang, J. *J. Am. Chem. Soc.* **2011**, *133*, 4330.
(64) Troisi, L.; Pindinelli, E.; Strusi, V.; Trinchera, P. *Tetrahedron: Asymmetry* **2009**, *20*, 368.
(65) Bose, A. K.; Chawla, H. P. S.; Dayal, B.; Foleys, D. A. *Org. Magn. Reson.* **1976**, *8*, 151.